ARTICLE IN PRESS – J. Appl. Cryst.

JOURNAL OF APPLIED CRYSTALLOGRAPHY

ISSN 1600-5767

Implementation of a self-consistent slab model of bilayer structure in the *SasView* suite

Proof instructions

Proof corrections should be returned by **30 December 2020**. After this period, the Editors reserve the right to publish your article with only the Managing Editor's corrections.

Please
(1) Read these proofs and assess whether any corrections are necessary.
(2) Check that any technical editing queries highlighted in **bold underlined** text have been answered.
(3) Send corrections by e-mail to **ls@iucr.org**. Please describe corrections using plain text, where possible, giving the line numbers indicated in the proof. Please do not make corrections to the pdf file electronically and please do not return the pdf file. If no corrections are required please let us know.

To arrange payment for **open access**, please visit **http://scripts.iucr.org/openaccess/?code=ei5065**. To purchase printed offprints, please complete the attached order form and return it by e-mail.

Please check the following details for your article

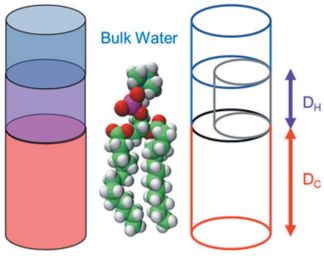

Thumbnail image for contents page

Synopsis: A self-consistent slab model for small-angle scattering data interpretation of bilayer structures has been implemented within the *SasView* software suite, and its application to the example of a lipid bilayer is demonstrated.

Abbreviated author list: Tan, L. (0000-0003-1809-815X); Elkins, J.G.; Davison, B.H.; Kelley, E.G. (0000-0002-6128-8517); Nickels, J. (0000-0001-8351-7846)

Keywords: lamellar phase; small-angle neutron scattering; SANS; small-angle X-ray scattering; SAXS; area per lipid; hydration number; lipids; membranes; block copolymers; liquid crystals

How to cite your article in press

Your article has not yet been assigned page numbers, but may be cited using the doi:

Tan, L., Elkins, J.G., Davison, B.H., Kelley, E.G. & Nickels, J. (2021). *J. Appl. Cryst.* **54**, https://doi.org/10.1107/S1600576720015526.

You will be sent the full citation when your article is published and also given instructions on how to download an electronic reprint of your article.

JOURNAL OF APPLIED CRYSTALLOGRAPHY
ISSN 1600-5767

Received 12 October 2020
Accepted 23 November 2020

Edited by F. Meilleur, Oak Ridge National Laboratory, USA, and North Carolina State University, USA

Keywords: lamellar phase; small-angle neutron scattering; SANS; small-angle X-ray scattering; SAXS; area per lipid; hydration number; lipids; membranes; block copolymers; liquid crystals.

Supporting information: this article has supporting information at journals.iucr.org/j

Implementation of a self-consistent slab model of bilayer structure in the *SasView* suite

Luoxi Tan,[a] James G. Elkins,[b] Brian H. Davison,[b] Elizabeth G. Kelley[c] and Jonathan Nickels[a]*

[a]Department of Chemical and Environmental Engineering, University of Cincinnati, 2901 Woodside Drive, Cincinnati, OH 45221, USA, [b]Biosciences Division, Oak Ridge National Laboratory, PO Box 2008, Oak Ridge, TN 37831, USA, and [c]Center for Neutron Research, National Institute of Standards and Technology, Gaithersberg, MD 20899, USA. *Correspondence e-mail: jonathan.nickels@uc.edu

Slab models are simple and useful structural descriptions which have long been used to describe lyotropic lamellar phases, such as lipid bilayers. Typically, slab models assume a midline symmetry and break a bilayer structure into three pieces, a central solvent-free core and two symmetric outer layers composed of the soluble portion of the amphiphile and associated solvent. This breakdown matches reasonably well to the distribution of neutron scattering length density and therefore is a convenient and common approach for the treatment of small-angle scattering data. Here, an implementation of this model within the *SasView* software suite is reported. The implementation is intended to provide physical consistency through the area per amphiphile molecule and number of solvent molecules included within the solvent-exposed outer layer. The proper use of this model requires knowledge of (or good estimates for) the amphiphile and solvent molecule volume and atomic composition, ultimately providing a self-consistent data treatment with only two free parameters: the lateral area per amphiphile molecule and the number of solvent molecules included in the outer region per amphiphile molecule. The use of this code is demonstrated in the fitting of standard lipid bilayer data sets, obtaining structural parameters consistent with prior literature and illustrating the typical and ideal cases of fitting for neutron scattering data obtained using single or multiple contrast conditions. While demonstrated here for lipid bilayers, this model is intended for general application to block copolymers, surfactants, and other lyotropic lamellar phase structures for which a slab model is able to reasonably estimate the neutron scattering length density/electron-density profile of inner and outer layers of the lamellae.

1. Introduction

Small-angle scattering is one of the primary techniques to investigate the transverse and lateral structure of lipid bilayers (Büldt *et al.*, 1979; Nickels, Chatterjee, Stanley *et al.*, 2017; Rand & Luzzati, 1968; Zaccai *et al.*, 1975, 1979) and other lyotropic lamellar phases, such as block copolymers (Sanson *et al.*, 2011), surfactants (Nallet *et al.*, 1993) and liquid crystals (Kekicheff *et al.*, 1984). This stems from the confluence of many bilayer thicknesses – 4 to 5 nm (Gennis, 2013) – with the probe length of small-angle scattering techniques (hundreds of nm to fractions of an nm), as well as the strong scattering contrast provided by many bilayer systems.

The level of structural detail required is a main consideration in the selection of a model and importantly in the acquisition of a scattering data set. For instance, small-angle X-ray scattering (SAXS) is an excellent option to obtain information about the thickness or repeat spacing of the lamellar phase in systems which have high-atomic-number

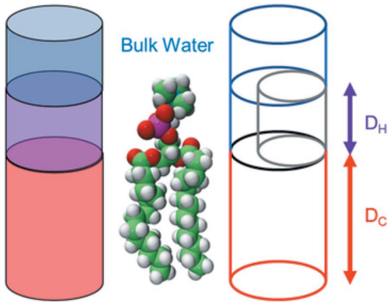

elements in characteristic locations, such as phosphorus in many lipid head groups (Zhang *et al.*, 1994; McIntosh & Simon, 1986; Lewis & Engelman, 1983*b*). These atoms give strong characteristic peaks in SAXS data which readily provide the spacing of phosphate groups for comparative thickness purposes, commonly referred to as D_{HH} (Kučerka *et al.*, 2011), as well as the lamellar repeat spacing if present. From these observations the full thickness of the bilayer, commonly D_B (Luzzati & Husson, 1962), and water content between the layers can be assessed. Fitting of the full electron-density (ED) profile is also possible (Bouwstra *et al.*, 1993) but fit results are often quite unsatisfying with only a single data set. Similar analysis schemes are possible for block copolymer systems where the water content of the outer layer is an important part of describing the 'polymer brush' (Radjabian *et al.*, 2017; Nunes, 2016; Meier *et al.*, 2000).

Small-angle neutron scattering (SANS) is perhaps more amenable to the study of the transverse structure due to its sensitivity to the neutron scattering length density (SLD), a property that varies by element and isotope. Whereas X-ray scattering reflects the ED of the sample, a property that systematically increases with atomic number, the SLD does not monotonically increase with atomic number. In this way, light elements common to soft materials, specifically hydrogen, contribute more strongly to the SLD profile of the bilayer. The resulting scattering pattern is therefore more indicative of the structure and distribution of molecules throughout the bilayer. In the case of lipids this means a clear indication of the thickness of the hydrophobic core, $2D_C$, and overall bilayer thickness. This full thickness of the bilayer can be broken down to the hydrocarbon thickness of the lipid tails, $2D_C$, and two headgroup thicknesses, D_H, which contain the lipid head group itself and associated water (Kučerka *et al.*, 2011). Another capability of neutron scattering is the possibility of isotopic substitution of natural abundance hydrogen (99.985% ^{1}H) with its isotope ^{2}H, or deuterium, in the bilayer or solvent. This can significantly alter the SLD profile without changing the structure, enabling multiple simultaneous measurements of the same structure with differing SLD profiles. This is extremely useful for simultaneous data fitting as we illustrate below. Simultaneous fitting can also be done in combination with X-ray scattering data to further constrain structural models during data fitting (Wiener & White, 1991; Kučerka *et al.*, 2008).

The interpretation of the resulting scattering patterns is now widely accessible with the help of publicly released data fitting software such as *SasView* (Doucet *et al.*, 2019), along with many undistributed investigator-driven models of varying levels of complexity. The simplest of these are based on slab models, also called strip models, which have long been used to describe lamellar structures (Worthington, 1969). In these models, the physical size of the bilayer is approximated by a 'slab' of defined thickness and average neutron scattering length density/electron density (SLD/ED). This is then transformed via a Fourier transform into the reciprocal space where it can be compared directly with scattering data; at this point curve fitting algorithms are able to match thickness and scattering contrast of the bilayer/solvent. This model is implemented in the current version of *SasView* as the aptly named 'lamellar' model (Berghausen *et al.*, 2001; Nallet *et al.*, 1993). Several variants of this model are also included, such as the 'lamellar_hg' model which introduces additional slabs to represent distinct outer/headgroup layers of the lamellar structure (Berghausen *et al.*, 2001; Nallet *et al.*, 1993). This allows the user to more accurately represent the inner/outer layer structures with separate thicknesses and scattering densities. Multilayer assemblies can also be analysed via the introduction of a structure factor and Caille parameter (Nallet *et al.*, 1993), while the spherical shape/size of a vesicle can be introduced from a variant of the sphere model (Guinier & Fournet, 1955). The 'core–shell'-type model can reproduce the inner/outer layering of the lamellar structures in spherical particles (Kline, 2006; Feigin & Svergun, 1987). The common outputs of these models are a physical thickness of the lamellae or layer and an associated SLD/ED. While these models provide useful parameters and may be sufficient detail for some analyses, there is no constraint within current versions of these models that forces the calculated parameters to be physically consistent with themselves in terms of the geometry and scattering length considerations. Therefore, these models may provide fits which are numerically valid, but the calculated parameters are inconsistent with each other, compromising their use in driving deeper physical insights. We provide a demonstration of this inconsistency in the supporting information Section S1. There we perform a fit on the data we discuss later using the existing 'lamellar_hg' function in the *SasView* suite. A good fit to the data is obtained and the resulting structure seems reasonable, except that one obtains different values for the water content of the outer layer depending if one uses the thickness of the head group or the SLD of the headgroup region as the basis for the calculation.

There is ultimately no limit to the shape or number of slabs used in modelling the SLD/ED profile of a bilayer. One might consider imposing linear dependences of the SLD/ED between the slabs (Kučerka *et al.*, 2004) to make the transitions between slabs less abrupt or imposing other functional forms, such as Gaussian functions, to obtain a semi-continuous SLD/ED profile (Rand & Luzzati, 1968). Associating these functional forms to the underlying chemistry of the amphiphile is a logical step to obtain more detailed structural information and has been implemented in the case of some lipids based on a variety of strategies for defining the partial volume/density of specific atoms or functional groups (Wiener & White, 1992; Armen *et al.*, 1998; Hub *et al.*, 2007; Kučerka *et al.*, 2008; Fogarty *et al.*, 2015), more details of which are reviewed elsewhere (Heberle *et al.*, 2012). This type of model is often readily comparable with the output of MD [**molecular dynamics?**] simulations (Nickels & Katsaras, 2019; Hub *et al.*, 2007) using code such as *SIMtoEXP* (Kučerka *et al.*, 2010) or *Sassena* (Lindner & Smith, 2012). There are of course caveats with such complex models. Firstly, such complex models are highly dependent upon the availability and quality of appropriate parameters for partial volume and SLD/ED of the

various regions defined in the parsing scheme. The choice of parsing scheme, functional form and other constraints such as molecular connectivity or total volume conservation is quite system specific and non-trivial to construct. Issues of inherent information content of scattering patterns with respect to the number of imposed structural features are relevant as well, especially for multicomponent systems where parameters needed to describe the structure are rapidly multiplied by the number of components. This is a concern which can sometimes be addressed with the simultaneous fitting of scattering data from different SLD/ED contrast conditions (Kučerka *et al.*, 2008). Finally, it should be noted that, to the best of our knowledge, a user-friendly software to implement models of this type is not currently available to the community for download. These caveats suggest that there are many occasions when one might find it more practical or advantageous to utilize more simple and robust slab models to describe a bilayer structure at lower resolution. Situations which come to mind might include bilayers with uncommon, or unparameterized, compositions, or heterogeneous composition like lipid extracts (Nickels, Chatterjee, Mostofian *et al.*, 2017) or live cells (Nickels, Chatterjee, Stanley *et al.*, 2017). Indeed, parameterization may prove more tractable given that total molecular volume and hydrophobic region volume estimates are often simpler to obtain and more reliable with small relative errors – further motivating the choice of parsing scheme in this work

The implementation of the existing slab models can be improved to address the shortcomings described above by imposing constraints specific to the molecular composition of the lamellar structure to reduce the number of free parameters to be varied in the fit algorithm to two: the area per lipid/molecule (APL) and the number of water or other solvent molecules contained within the outer/headgroup region (n_W). Recapping, the simpler parsing scheme is based on two layers with assumed central symmetry: a solvent-free inner layer and a solvent-containing outer layer, all surrounded by the bulk solvent (Kučerka *et al.*, 2004; Worthington, 1969; Feigin & Svergun, 1987; Nagle & Wiener, 1988). Rendering these volumes as homogeneous slabs, we can generate an SLD profile approximating that of the bilayer in some cases. Fig. 1 illustrates the general parsing of an example lipid bilayer 1,2-dimyristoyl-*sn*-glycero-3-phosphocholine into a core layer comprised of the lipid tails. Beginning with the geometry, the volume, V_C, of the inner layer portion of the amphiphile can be related to the inner layer thickness, D_C, and the APL via $D_C \times \mathrm{APL} = V_C$. The outer layer is then comprised of the lipid head group and associated water, with the per amphiphile volume in the outer layer defined as $V_H = V_{HL} + n_W \times V_W$ and $D_H \times \mathrm{APL} = V_H$, where V_H is combined solvent and amphiphile volume in the outer layer, V_{HL} the amphiphile portion in the outer layer, n_W the number of solvent molecules per amphiphile in the outer layer, and V_W the molecular volume of one solvent molecule. D_H is the outer layer thickness. It should be understood that the water profile will have an impact upon the appropriateness of this model for any given system. As we will show here for lipids, our model returns a full steric thickness that reflects the full extent of the head group and associated water, larger than the commonly discussed parameter D_B, though D_B can, of course, still be computed from V_L [$\underline{V_{HL}}$**?**] and the APL.

The SLD of each layer is to be estimated by dividing the summed scattering length of the atoms within the layer on a per amphiphile basis, by the volume of the contents, again on a per amphiphile basis. For example, the SLD of the inner layer of a lipid bilayer is defined as the second carbon of the lipid tail, as water penetration is limited to the level of the ester bonds (Nagle & Wiener, 1988; Wiener *et al.*, 1988; Nagle & Tristram-Nagle, 2000; Nickels & Katsaras, 2015; Zaccai *et al.*, 1975; Rand & Parsegian, 1989). This means we define the scattering length of the atoms in the lipid tails beyond the second carbon on both chains and divide by the molecular volume of the two acyl chains. Similarly, in the outer layer, the SLD would be the sum of the scattering length of the head group and associated water divided by the volume of the outer layer on a per amphiphile basis ($\mathrm{SLD_H} = b_H + n_W \times b_W)/V_H$. Fig. 1 also denotes neutron SLD of these regions on a red to blue scale for the case of natural abundance hydrogen containing lipid in D_2O as well as the key equations used to define the SLD. The same two variables, n_W and APL, are required to solve for the bilayer thickness and the SLD to define the SLD profile and fit our scattering data.

These relations establish a constraint in our data fitting which we can use to enforce self-consistency. We provide the

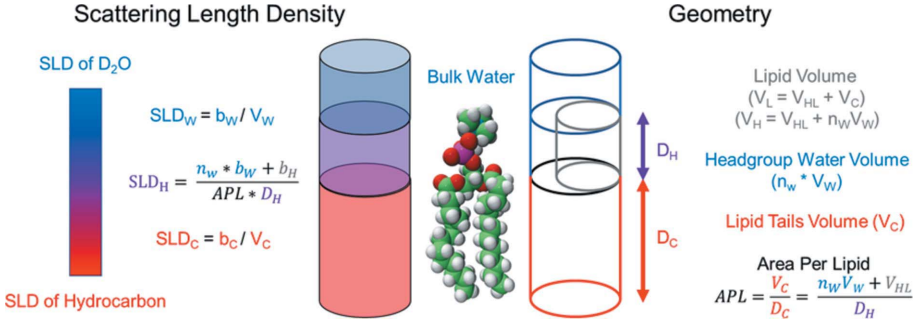

Figure 1
Slab model and associated relationships to establish self-consistency by constraining the molecular volumes shown here for the case of a lipid bilayer. The model should be parameterized by the molecular volumes and sum of atomic scattering lengths for the respective regions. The parsing scheme is based on a solvent-free inner layer, an outer layer containing both the solvent-exposed portion of the amphiphile and associated water. The associated partial molecular volumes, solvent volumes and scattering lengths provide geometric and SLD constraints. The area per lipid (area per amphiphile), APL, and number of water (solvent) molecules per amphiphile, n_W, should be allowed to vary in the fitting algorithm. From the APL, n_W and molecular volumes, the thickness of the head and tail regions can be calculated.

associated Python code to be implemented in the *SasView* suite as supporting information. This implementation is intended to be used when one has good knowledge of, or estimates for, the molecular volume of the amphiphile in each region, V_L, V_{HL} and V_C, and solvent, V_W, along with a clear understanding of the associated atomic compositions so one can compute the summed scattering lengths, b_{HG}, b_{Tails}, b_W. Below we discuss the application of this model to scattering data obtained from model lipid bilayers, demonstrating the typical case of a hydrogenated lipid in deuterated solvent, along with a more ideal case of simultaneous fitting of multiple contrast conditions for the same model lipid bilayer sample.

2. Methods

2.1. Sample preparation

Lipid materials were obtained from Avanti Polar Lipids (Alabaster, AL). Natural abundance hydrogen lipids used include 1,2-dimyristoyl-*sn*-glycero-3-phosphocholine (DMPC), 1,2-dipalmitoyl-*sn*-glycero-3-phosphocholine (DPPC) and 1,2-distearoyl-*sn*-glycero-3-phosphocholine (DSPC). Deuterated lipids used were tail-deuterated DMPC, d54-1,2-dimyristoyl-*sn*-glycero-3-phosphocholine (d54-DMPC) and tail-deuterated DSPC, d70-1,2-distearoyl-*sn*-glycero-3-phosphocholine (d70-DSPC). Vesicle samples were prepared for natural abundance hydrogen materials by first dissolving lipid materials in chloroform, then drying the solution to form a lipid film. Lipid mixtures were also prepared with tail-deuterated lipids in a 90% D/10% H lipid to match the SLD of 100% D_2O by first combining the chloroform solutions before drying under nitrogen to a homogeneous film. Films were hydrated with the selected solvent and extruded using mini extruders from Avanti Polar Lipids (Alabaster, AL) at a temperature above the melting transition, using 400, 200 and 100 nm pore membranes sequentially to yield monodisperse lipid vesicles ~100 nm in diameter.

2.2. Small-angle neutron scattering (SANS)

SANS experiments were performed at the National Institute of Standards and Technology (NIST) Center for Neutron Research on the NG7 and NGB30 30 m SANS instruments. Measurements were performed using a neutron wavelength λ = 6 Å with a wavelength distribution $\Delta\lambda/\lambda$ = 0.12 and using sample-to-detector distances of 1, 4 and 13 m to access a q range of 0.002–0.45 $Å^{-1}$. The magnitude of the scattering vector, q, is defined as $q = 4\pi/\lambda = \sin(\theta/2)$ where θ is the scattering angle. The temperature was controlled within +0.1°C and the samples were equilibrated for at least 15 min before starting the measurements. The data for the samples were corrected for the empty cell and background scattering as well as the detector sensitivity using the *IGOR* macros provided by NIST (Kline, 2006).

Data fitting was performed in the *SasView* suite (Doucet *et al.*, 2019), using the self-consistent slab model described in this work. The code to implement this model fit is included in the supporting information with the filename 'lamellar_slab_APL_nW.py'. Fits were performed for the DPPC in D_2O data set as a single fit. Single fits were performed for each contrast condition, as well as simultaneous linked fits for pairs, or all three data sets as specified in the text for DMPC and DSPC. The fitting was performed in the q range of 0.02–0.4 $Å^{-1}$ using the *DREAM* algorithm as the fitting engine (Vrugt *et al.*, 2008). Literature or calculated values were entered and held constant for the following parameters: headgroup volume and scattering length, the acyl tails' volume and scattering length, and water's volume and scattering length. The scale factor, background, APL and n_W were allowed to vary in the fits.

3. Results and discussion

To demonstrate the model, two groups of SANS measurements were made on model lipid bilayers. Firstly, we have measured a typical hydrogenated PC [**phosphocholine?**] lipid bilayer in D_2O (DPPC, Fig. 2). This represents a typical measurement with reasonable contrast between the inner,

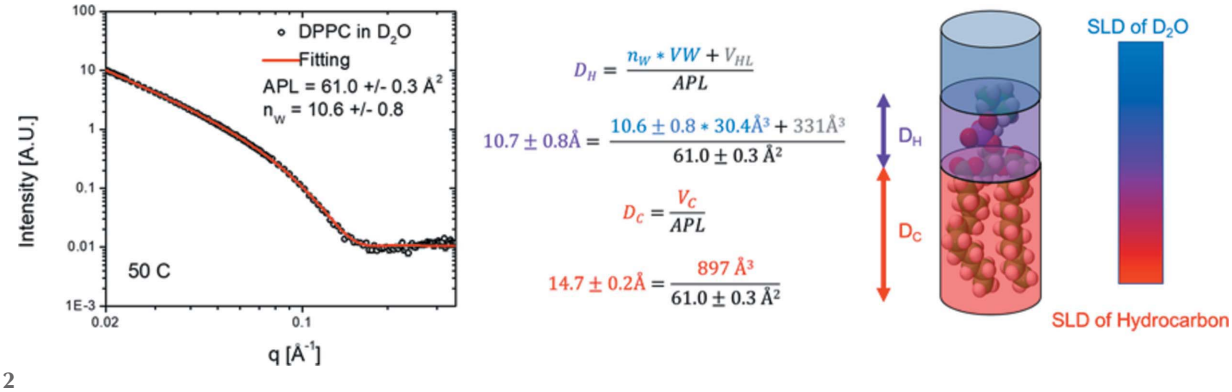

Figure 2
SANS data and fit curves for DPPC lipid bilayer in D_2O at 50°C using the self-consistent lamellar slab model 'lamellar_Slab_APL_nW' implemented in *SasView* (code included in the supporting information). The fit to the data provides the APL and n_W from which we can derive structural description of the bilayer using the relations shown. Error is reported as a 95% confidence interval throughout the article.

Table 1
Molecular volumes (Tristram-Nagle *et al.*, 2002; Kučerka *et al.*, 2011) and scattering lengths (Sears, 1992) used in fitting of scattering data.

1 fm = 10 × 10^{-15} m.

	DMPC	DPPC	DSPC
V_{HG} (Å^3)	331	331	331
V_{Tails} (Å^3)	769	897	1017
V_W (Å^3)	30.4	30.4	30.4
b_{HG} (fm)	60	60	60
b_{Tails} (fm)	−29.2	−32.5	−35.9
$b_{Tails\ (90\%\ D/10\%\ H)}$ (fm)	476.9		620.1
$b_{W\ (0\%\ D)}$ (fm)	−1.7		−1.7
$b_{W\ (35\%\ D)}$ (fm)	5.6		5.6
$b_{W\ (100\%\ D)}$ (fm)	19.2	19.2	19.2

outer and solvent layers. Secondly, we present a set of measurements on DMPC and DSPC bilayers at three distinct contrast conditions for each lipid (Fig. 3). The lipids in the second case are a mixture of 90% (mol.%) tail-deuterated–10% (mol.%) natural abundance hydrogen content to match the tail region of the lipids to the SLD of pure D_2O. Two other solvent conditions were used: 0% D_2O, generating contrast between all layers, and 35% D_2O, matching the SLD of the choline head group. Each measurement in the second set of data would be challenging to fit on its own, with significant covariance leading to poor fits, but when taken in combination and fitted simultaneously using this model, high-quality structural information can be obtained.

Parameterization of the model is of great importance to the resulting structural description. Accurate molecular volumes and scattering length values must be combined with a parsing scheme which achieves a good compromise between physically meaningful boundary and maximal contrast between layers of roughly even SLD. In the case of the PC lipids that we examine here, there is a mature body of literature from which we can find these values, and include as Table 1 (Tristram-Nagle *et al.*, 2002; Kučerka *et al.*, 2011; Sears, 1992). There is a degree of variability in the values reported in the literature. For instance, PC headgroup volumes of 331 Å^3 (Tristram-Nagle *et al.*, 2002) or 319 Å^3 (Sun *et al.*, 1994) have been reported. Lipid volumes also vary somewhat, for example DMPC volumes ranging from 1094 Å^3 to 1101 Å^3 are reported (Nagle & Wilkinson, 1978; Petrache *et al.*, 2000; Schmidt & Knoll, 1985). This, in conjunction with different input data and methodologies, leads to some degree of variation in the observed structural parameters of lipid bilayers as noted below. It is also common to use volume estimates for portions of the molecule, such as a methylene unit or phosphate group. One can then sum the various pieces contained in the region to which it is assigned (Armen *et al.*, 1998).

The fit of SANS data from a DPPC vesicle sample in D_2O, measured at 50°C, is shown in Fig. 2. The fit did converge, and we see a close agreement of the model and the SANS data (Fig. S1). Our fit of the scattering data yielded both an estimate of 61.0±0.3 Å for APL and 10.6±0.8 water molecules per lipid. This fitting is based upon the parameters chosen for molecular volume from the literature for DPPC and scattering length data tabulated by Sears (Tristram-Nagle *et al.*, 2002; Kučerka *et al.*, 2011; Sears, 1992) and the result would vary if other literature values were chosen. Again, we used a parsing scheme with a boundary at the C2 carbon of the acyl tail, resulting in a volume for the two acyl tails of the lipid of 897 Å^3 and a headgroup volume of 331 Å^3, with a water volume of 30.4 Å^3. The scattering lengths of these regions

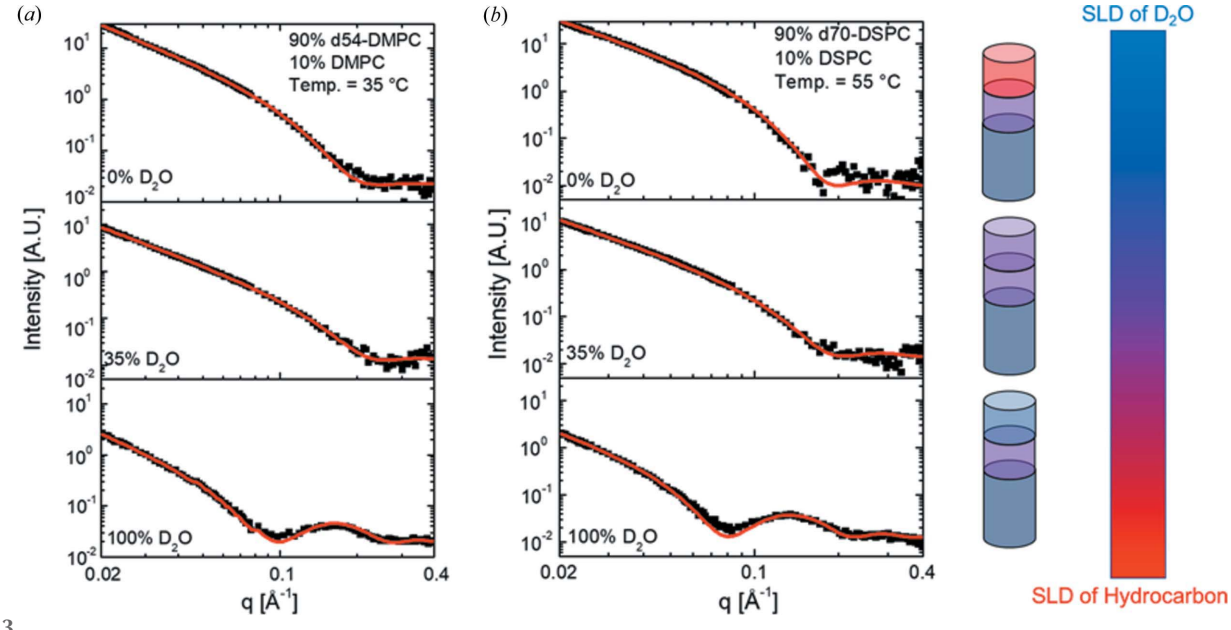

Figure 3
SANS data and fit curves for a simultaneous fitting of three contrast conditions of (*a*) DMPC at 35°C and (*b*) DSPC at 55°C using the self-consistent lamellar slab model implemented in *SasView* (code included in the supporting information). The different contrast conditions depicted as a colour scale to the right of the figures show how contrast variation results in three distinct scattering patterns for the same sample by varying the H_2O/D_2O ratio in the solvent, a technique amenable to simultaneous data fitting.

were −32.5 fm, 60 fm and 19.2 fm, respectively. In Table 1, we provide the values used in our fitting of DPPC and our subsequent treatment of DMPC and DSPC.

The value of APL obtained (61.0±0.3 Å [**add superscript 2 to Å?**], reported as a 95% confidence interval for values from our fits throughout) is in good agreement with prior reports in the literature for DPPC which vary from ∼61 Å^2 (Balgavý *et al.*, 2001) to 66.5 Å^2 (Lewis & Engelman, 1983*a*), with other commonly cited reports of 63.1±1.3 Å^2 (reporting one standard deviation) (Kučerka *et al.*, 2011), 64.0 Å^2 (Nagle & Tristram-Nagle, 2000), 63.3 Å^2 (Petrache *et al.*, 2000) and 63.8±0.7 Å^2 (Fogarty *et al.*, 2015). From the current values of APL and n_W, we can compute the hydrocarbon thickness, $2D_C$, if we involve the partial molecular volume for the lipid tails, obtaining a hydrophobic thickness of 29.4±0.4 Å. This derived value shows similar agreement, with reported $2D_C$ values for DPPC ranging from 26 Å (Lewis & Engelman, 1983*a*) to 28.4 Å (Petrache *et al.*, 2000) to 28.5±0.6 Å (reporting one standard deviation) (Kučerka *et al.*, 2011) to 30 Å (Nagle & Tristram-Nagle, 2000). The total bilayer thickness obtained in our model is 50.8±2.9 Å, somewhat larger than other reports of lipid bilayer thickness reported as D_B. This has to do with the definition of D_B (Luzzati & Husson, 1962) which is $D_B = V_L/\mathrm{APL}$. This is an extremely useful quantity in the case of **MLV [please define]** samples where water content can be inferred from D_B and the repeat spacing. In the case of single bilayer modelling, it is less practical except in its approximation of the phosphate group spacing obtained from X-ray scattering measurements (often found as D_{HH}). If we compute D_B in this way, we obtain a value of D_B = 39.9±0.4 Å, in reasonable agreement with literature reports, 39.0±0.8 Å (reporting one standard deviation) (Kučerka *et al.*, 2011). For this case, the thickness of the reported bilayer slabs will include the water associated with the amphiphile. In this way one might report D_B for consistency and comparison with prior work or consider the full slab thickness to capture the head group and its interaction with the solvent better.

The second set of measurements (for DMPC and DSPC) have been made at three different solvent contrast conditions (0% D_2O, 35% D_2O and 100% D_2O) for each lipid using tail-deuterated lipids (90%/10% H/D lipid) (Fig. 3). As we show above, typically it is best to use contrast conditions in which each layer, the tails (core), head groups (outer layer) and solvent, all possess distinct SLDs and the incoherent background of neutron scattering is minimized by using a high fraction of deuterated solvent. Here, we look at these three contrast conditions which do not meet these criteria on their own, but which in combination can provide quality structural information. Simultaneous fitting is a feature in the *SasView* program which allows one to apply a minimization algorithm to one unified structural model across multiple data sets. The case of headgroup matching is actually useful for studies focused only on the thickness or organization of the hydrophobic core (Nickels *et al.*, 2015). It is also convenient for the study of the cell membrane in the special case of living systems which is contrast matched to the solvent and contrast introduced only in the hydrophobic core of the membrane (Nickels, Chatterjee, Stanley *et al.*, 2017; Nickels, Chatterjee, Mostofian *et al.*, 2017). Contrast matching the core and solvent regions is particularly useful for another special case, isolating thickness fluctuations via other advanced scattering techniques (Woodka *et al.*, 2012). Also included is the 0% D_2O condition, which does present layers of distinct SLD, but is plagued by the high incoherent scattering background from H_2O in the solvent.

Table 2
Results of data fitting using our self-consistent lamellar model for bilayer structure.

Values shown for DPPC in D_2O single fit, and DMPC and DSPC from the three-curve simultaneous fit.

	DMPC	DPPC	DSPC
Temperature (°C)	35	50	55
APL (Å^2)	62.9±0.3	61.0±0.3	66.9±0.2
n_W	9.9±0.4	10.6±0.3	14.1±0.4
$2D_C$ (Å)	24.4±0.2	29.4±0.2	30.4±0.2
D_B (Å)	34.9±0.3	40.3±2.9	41.8±1.4

It can be seen in Fig. 3 that our model replicates the data quite well for both lipids when applied as a simultaneous fit over all three contrast conditions (the covariance matrix for each fit can be found in Figs. S2 and S3). The resulting structural parameters for both lipids are physically reasonable and consistent with prior work. For DMPC we obtain an estimated APL of 62.9±0.3 Å^2 and n_W of 9.9±0.4. From this we calculate a hydrocarbon thickness of 24.4±0.2 Å and estimate D_B at 34.9±0.3 Å. For DSPC we obtain an estimated APL of 66.9±0.2 Å^2 and n_W of 14.1±0.4. From this we calculate a hydrocarbon thickness of 30.4±0.2 Å and estimate D_B at 39.5±0.2 Å. Reported values of APL for DMPC vary from ∼59.3 Å^2 (Balgavý *et al.*, 2001) to 65.7 Å^2 (Lewis & Engelman, 1983*a*), with other commonly cited values of 59.9±1.2 Å^2 (Kučerka *et al.*, 2011), 64.0 Å^2 (Nagle & Tristram-Nagle, 2000) and 60.0 Å^2 (Petrache *et al.*, 2000). Our derived values for hydrophobic thickness show a similar agreement, with reported $2D_C$ values ranging from 23 Å (Lewis & Engelman, 1983*a*) to 25.6 Å (Petrache *et al.*, 2000) to 25.7±0.6 Å (Kučerka *et al.*, 2011) to 26.2 Å (Nagle & Tristram-Nagle, 2000). DSPC literature values for APL vary from ∼63.8±1.3 Å^2 (Kučerka *et al.*, 2011) to 67.2 Å^2 (Balgavý *et al.*, 2001). Hydrophobic thickness values for DSPC show a similar agreement, with reported $2D_C$ values ranging from 29.5 Å (Lewis & Engelman, 1983*a*) to 31.2 Å (Petrache *et al.*, 2000) to 31.9±1.3 Å (Kučerka *et al.*, 2011). A summary and comparison of all three lipid structures DMPC, DPPC and DSPC can be found in Fig. 4 and Table 2.

We also include an extrapolation of the hydrophobic thickness, $2D_C$, to a common temperature of 60°C. This is done using the thermal expansion coefficient (Petrache *et al.*, 2000). Extrapolating these values to a common temperature permits us to compare more directly across different hydrocarbon chain lengths and obtain an estimate of the CH_2 group volume. $2D_C$ was found to vary systematically for these PC lipids with increasing acyl chain length as expected: 23.2 Å for DMPC,

28.6 Å for DPPC and 30.0 Å for DSPC. Plotting this as a function of carbons in the acyl chain, we can use ΔD_C times the APL, divided by the difference in number of methylene units to obtain an estimate of the CH_2 volume, obtaining a value of V_{CH2} = 28.3±1.1 Å^3 (95% confidence interval). This value compares favourably with literature reports of V_{CH2} as 28.4 Å^3 (Nagle & Tristram-Nagle, 2000) and 28.1 Å^3 (Armen *et al.*, 1998).

As noted above, the three contrast conditions do not necessarily constitute a good data set on their own; indeed each one is flawed in this case. The 0% D_2O contrast condition is compromised by the high incoherent background, the 35% D_2O sample contains no contrast between the headgroup region and the solvent, and the 100% D_2O condition presents no contrast between the acyl core and the solvent. We have fitted each of these curves independently and as pairs for DMPC and DSPC and include the results in Table S1 and Table S2. The data and fitted curves are available in Figs. S4–S7. Here, we see how the model is able to reproduce the data set in all cases but provides structural values which are nonsensical from any understanding of the sample. Beginning with the 0% D_2O sample, we see that the large incoherent scattering obscures the high-q portion of the curve and results in a poor fit. The 35% D_2O sample presents as only one layer, with the head group and solvent contrast matched. As such, the model fits the hydrophobic thickness quite well and completely fails to describe the outer layer as the water content does not impact the SLD. This is precisely what we observe for both DMPC and DSPC, D_C values in close agreement with the simultaneous fit (24.4±0.2 Å versus 24.7±0.4 Å for DMPC and 30.4±0.2 Å versus 32.0±0.5 Å for DSPC, reporting 95% confidence interval). The 100% D_2O curves present as only the headgroup region, without any contrast between the solvent and hydrophobic core. This model now has no way of recognizing the appropriate thickness of the head group with respect to the hydrophobic core. This results in a reasonable value of D_B but APL and n_W values which are artifactual. The covariance plots in Figs. S4–S7 are very instructive in understanding how the model compensates for ill-defined data. Narrow diagonal lines in these plots indicate that two variables compensate for each other in a direct way. The simultaneous fitting of pairs of contrast conditions improves the data fitting by forcing the model to consider combinations of data which reflect different pieces of the structure well, while not providing sufficient information on their own.

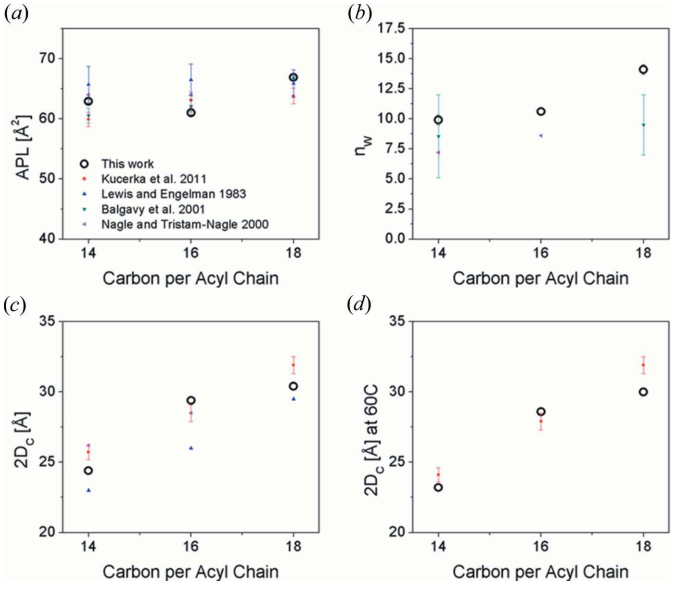

Figure 4
Structural parameters obtained using the self-consistent lamellar model, 'lamellar_slab_APL_nW' as a function of carbon atoms in the acyl tail of the PC lipid. Here we show the comparison of our results for the single fit of DPPC in D_2O and simultaneous fitting of all three DMPC or DSPC data sets with prior work (Balgavý *et al.*, 2001; Kučerka *et al.*, 2011; Lewis & Engelman, 1983*a*; Nagle & Tristram-Nagle, 2000). The obtained values are in reasonable agreement. Note that $2D_C$ at 60°C values were extrapolated using previously reported thermal expansion coefficients (Petrache *et al.*, 2000).

4. Related literature

The following reference is cited in the supporting information: Tan *et al.* (2020).

5. Conclusions

The structure of lipid bilayers and other lyotropic lamellar phases is of great importance for a variety of fields. Here, we provide a structural model based on homogeneous slabs, representing the structure as a solvent-free inner layer and solvent-containing outer layer. This breakdown matches reasonably well to the distribution of neutron SLD in many lamellar systems and therefore may be an appropriate and convenient approach for the treatment of small-angle scattering data. Because we parse the bilayer into two layers, we anticipate that the model will be of great use for heterogeneous bilayers such as multicomponent lipid bilayers, mixed block copolymer systems, lipid extracts, live cells – as well as in cases where it is sufficient to know the area per lipid (amphiphile), APL, total bilayer thickness, D_B, hydrocarbon core thickness, $2D_C$, headgroup/outer layer thickness, D_H, and/or water content n_W.

This model is an improvement upon the existing capabilities of the *SasView* suite because it provides the user with the opportunity to constrain the fit using the relevant molecular volumes and scattering lengths. We have provided the associated Python file to implement this model as a plugin within the small-angle scattering analysis suite, *SasView*. The use of this model was demonstrated with the fitting of SANS data for PC lipids. We first show a typical use of the model for a hydrogenated lipid in D_2O, before illustrating its use in a simultaneous fitting of three measurements collected at different contrast conditions. In both cases, the model produces structural descriptions in good agreement with literature reports. A series of fits are also included in the supporting information which illustrate how the model predictably fails as a result of data quality issues, and how combining such data sets using simultaneous fitting results in

quality fits nonetheless. Beyond lipid bilayers, we anticipate that this model will also serve the community in the treatment of scattering data from block copolymers, surfactants and other lyotropic lamellar phase structures.

Acknowledgements

Identification of any commercial products or trade names does not imply endorsement or recommendation by the National Institute of Standards and Technology.

Funding information

This research was supported by the Genomic Science Program, Office of Biological and Environmental Research, US Department of Energy (DOE), under Contract FWP ERKP752. This work benefited from the use of the *SasView* application, originally developed under NSF Award DMR-0520547. *SasView* also contains code developed with funding from the EU Horizon 2020 programme under the SINE2020 project grant No. 654000. Access to the NGB30 SANS Instrument was provided by the Center for High Resolution Neutron Scattering, a partnership between the National Institute of Standards and Technology and the National Science Foundation under Agreement No. DMR-2010792.

References

Armen, R. S., Uitto, O. D. & Feller, S. E. (1998). *Biophys. J.* **75**, 734–744.
Balgavý, P., Dubničková, M., Kučerka, N., Kiselev, M. A., Yaradaikin, S. P. & Uhríková, D. (2001). *Biochim. Biophys. Acta*, **1512**, 40–52.
Berghausen, J., Zipfel, J., Lindner, P. & Richtering, W. (2001). *J. Phys. Chem. B*, **105**, 11081–11088.
Bouwstra, J., Gooris, G., Bras, W. & Talsma, H. (1993). *Chem. Phys. Lipids*, **64**, 83–98.
Büldt, G., Gally, H., Seelig, J. & Zaccai, G. (1979). *J. Mol. Biol.* **134**, 673–691.
Doucet, M., Cho, J. H., Alina, G., Bakker, J., Bouwman, W., Butler, P., Campbell, K., Cooper-Benun, T., Durniak, C., Forster, L., Gonzales, M., Heenan, R., Jackson, A., King, S., Kienzle, P., Krzywon, J., Nielsen, T., O'Driscoll, L., Potrzebowski, W., Ferraz Leal, R., Rozycko, P., Snow, T. & Washington, A. (2019). *Zenodo.* **further details?**
Feigin, L. & Svergun, D. I. (1987). *Structure Analysis by Small-angle X-ray and Neutron Scattering.* **City of publication?**: Springer.
Fogarty, J. C., Arjunwadkar, M., Pandit, S. A. & Pan, J. (2015). *Biochim. Biophys. Acta*, **1848**, 662–672.
Gennis, R. B. (2013). *Biomembranes: Molecular Structure and Function.* **City of publication?**: Springer Science & Business Media.
Guinier, A. & Fournet, G. (1955). *Small-angle Scattering of X-rays.* London: Chapman & Hall?
Heberle, F. A., Pan, J., Standaert, R. F., Drazba, P., Kučerka, N. & Katsaras, J. J. (2012). *Eur. Biophys. J.* **41**, 875–890.
Hub, J. S., Salditt, T., Rheinstädter, M. C. & de Groot, B. L. (2007). *Biophys. J.* **93**, 3156–3168.
Kekicheff, P., Cabane, B. & Rawiso, M. (1984). *J. Phys. Lett.* **45**, 813–821.
Kline, S. R. (2006). *J. Appl. Cryst.* **39**, 895–900.
Kučerka, N., Katsaras, J. & Nagle, J. F. (2010). *J. Membr. Biol.* **235**, 43–50.
Kučerka, N., Nagle, J. F., Feller, S. E. & Balgavý, P. (2004). *Phys. Rev. E*, **69**, 051903.
Kučerka, N., Nagle, J. F., Sachs, J. N., Feller, S. E., Pencer, J., Jackson, A. & Katsaras, J. (2008). *Biophys. J.* **95**, 2356–2367.
Kučerka, N., Nieh, M.-P. & Katsaras, J. (2011). *Biochim. Biophys. Acta*, **1808**, 2761–2771.
Lewis, B. A. & Engelman, D. M. (1983*a*). *J. Mol. Biol.* **166**, 211–217.
Lewis, B. A. & Engelman, D. M. (1983*b*). **J Mol Biol? 166**, 211–217. **This reference appears to be the same as Lewis & Engelman 1983*a* above**
Lindner, B. & Smith, J. C. (2012). *Comput. Phys. Commun.* **183**, 1491–1501.
Luzzati, V. & Husson, F. (1962). *J. Cell Biol.* **12**, 207–219.
McIntosh, T. J. & Simon, S. A. (1986). *Biochemistry*, **25**, 4058–4066.
Meier, W., Nardin, C. & Winterhalter, M. (2000). *Angew. Chem. Int. Ed.* **39**, 4599–4602.
Nagle, J. & Wiener, M. (1988). *Biochim. Biophys. Acta*, **942**, 1–10.
Nagle, J. F. & Tristram-Nagle, S. (2000). *Biochim. Biophys. Acta*, **1469**, 159–195.
Nagle, J. F. & Wilkinson, D. A. (1978). *Biophys. J.* **23**, 159–175.
Nallet, F., Laversanne, R. & Roux, D. (1993). *J. Phys. II*, **3**, 487–502.
Nickels, J. D., Chatterjee, S., Mostofian, B., Stanley, C. B., Ohl, M., Zolnierczuk, P., Schulz, R., Myles, D. A., Standaert, R. F., Elkins, J. G., Cheng, X. & Katsaras, J. (2017). *J. Phys. Chem. Lett.* **8**, 4214–4217.
Nickels, J. D., Chatterjee, S., Stanley, C. B., Qian, S., Cheng, X., Myles, D. A., Standaert, R. F., Elkins, J. G. & Katsaras, J. (2017). *PLoS Biol.* **15**, e2002214.
Nickels, J. D., Cheng, X., Mostofian, B., Stanley, C., Lindner, B., Heberle, F. A., Perticaroli, S., Feygenson, M., Egami, T. & Standaert, R. F. (2015). *J. Am. Chem. Soc.* **Vol. and page numbers?**
Nickels, J. D. & Katsaras, J. (2015). *Subcell. Biochem.* **71**, 45–67.
Nickels, J. D. & Katsaras, J. (2019). *Characterization of Biological Membranes*, pp. 515. **City of publication?**: Walter de Gruyter GmbH & Co KG.
Nunes, S. P. (2016). *Macromolecules*, **49**, 2905–2916.
Petrache, H. I., Dodd, S. W. & Brown, M. F. (2000). *Biophys. J.* **79**, 3172–3192.
Radjabian, M., Abetz, C., Fischer, B., Meyer, A. & Abetz, V. (2017). *Appl. Mater. Interfaces*, **9**, 31224–31234.
Rand, R. & Parsegian, V. (1989). *Biochim. Biophys. Acta*, **988**, 351–376.
Rand, R. P. & Luzzati, V. (1968). *Biophys. J.* **8**, 125–137.
Sanson, C., Diou, O., Thévenot, J., Ibarboure, E., Soum, A., Brûlet, A., Miraux, S., Thiaudière, E., Tan, S., Brisson, A., Dupuis, V., Sandre, O. & Lecommandoux, S. (2011). *ACS Nano*, **5**, 1122–1140.
Schmidt, G. & Knoll, W. (1985). *Ber. Bunsen. Phys. Chem.* **89**, 36–43.
Sears, V. F. (1992). *Neutron News*, **3**, 26–37.
Sun, W.-J., Suter, R., Knewtson, M., Worthington, C., Tristram-Nagle, S., Zhang, R. & Nagle, J. (1994). *Phys. Rev. E*, **49**, 4665–4676.
Tan, L., Elkins J. G., Davison, B. H., Kelly, E. G. & Nickels, J. D. (2020). Submitted. **Any further update?**
Tristram-Nagle, S., Liu, Y., Legleiter, J. & Nagle, J. F. (2002). *Biophys. J.* **83**, 3324–3335.
Vrugt, J. A., Ter Braak, C. J., Clark, M. P., Hyman, J. M. & Robinson, B. A. J. W. R. R. (2008). **Journal name?**, **44**, **page numbers?**
Wiener, M., Tristram-Nagle, S., Wilkinson, D. A., Campbell, L. & Nagle, J. (1988). *Biochim. Biophys. Acta*, **938**, 135–142.
Wiener, M. C. & White, S. H. (1991). *Biophys. J.* **59**, 162–173.
Wiener, M. C. & White, S. H. (1992). *Biophys. J.* **61**, 434–447.
Woodka, A. C., Butler, P. D., Porcar, L., Farago, B. & Nagao, M. (2012). *Phys. Rev. Lett.* **109**, 058102.
Worthington, C. (1969). *Biophys. J.* **9**, 222–234.
Zaccai, G., Blasie, J. & Schoenborn, B. (1975). *Proc. Natl Acad. Sci. USA*, **72**, 376–380.
Zaccai, G., Büldt, G., Seelig, A. & Seelig, J. (1979). *J. Mol. Biol.* **134**, 693–706.
Zhang, R., Suter, R. M. & Nagle, J. F. (1994). *Phys. Rev. E Stat. Phys. Plasmas Fluids Relat. Interdiscip. Topics*, **50**, 5047–5060.